International Journal of Refrigeration 169 (2025) 226–240

Contents lists available at ScienceDirect

International Journal of Refrigeration

journal homepage: www.elsevier.com/locate/ijrefrig

INSTITUT INTERNATIONAL DU FROID
INTERNATIONAL INSTITUTE OF REFRIGERATION

Experimental comparison of cycle modifications and ejector control methods using variable geometry and CO_2 pump in a multi-evaporator transcritical CO_2 refrigeration system

Gabriele Toffoletti [a,b,*], Riley B. Barta [a], Steven M. Grajales [a], Haotian Liu [a], Davide Ziviani [a], Eckhard A. Groll [a]

[a] Ray W. Herrick Laboratories, School of Mechanical Engineering, Purdue University, West Lafayette, IN, USA
[b] University of Udine, Via Palladio, 8, 33100 Udine, Italy

ARTICLE INFO

Keywords:
Ejector control
Transcritical carbon dioxide
Transport refrigeration
Supermarket refrigeration
Economization

ABSTRACT

To reduce the direct global warming impact of refrigerants in HVAC&R applications, low-global warming potential (GWP) refrigerants, including natural refrigerants, have been extensively investigated as alternatives to hydrofluorocarbon (HFC) refrigerants. Among the natural refrigerants, Carbon Dioxide (CO_2) offers several advantages, such as excellent transport and thermo-physical properties, being neither toxic nor flammable, and having a low price and high availability around the world. However, the high critical pressure and low critical temperature of CO_2 often lead to transcritical operation, resulting in lower efficiency due to the additional compressor power necessary to achieve transcritical operation relative to subcritical HFC cycles. Therefore, a number of cycle modifications are used to enhance the coefficient of performance (COP) of transcritical CO_2 cycles to meet or surpass those of HFC cycles. This paper provides a systematic experimental investigation of four such cycle architectures by employing the same multi-stage, two-evaporator CO_2 refrigeration cycle test stand, 3 of these configurations in transcritical and 1 in subcritical conditions. The four cycles architectures included intercooling, open economization, an internal heat exchanger and two different ejector control approaches. Specifically, a variable-diameter motive nozzle and a variable-speed liquid CO_2 pump located directly upstream of the ejector motive nozzle inlet were analyzed. Based on the experimental data, the maximum COP improvements are 4.64 % and 9.47 % when the ejector and the internal heat exchanger are used, respectively. The CO_2 pump, once successfully stabilized, can control the ejector, increase its efficiency by up to 15 % and increase the cooling capacity to a maximum of 6.2 %. Nevertheless, a reduction in COP is measured when the pump is in use; however, unlike the other three different configurations, it was only analyzed under subcritical conditions.

1. Introduction

Since the revitalization of Carbon Dioxide (CO_2) as a refrigerant in the 1990s (Lorentzen, 1994), extensive research on increasing the efficiency of vapor compression cycles utilizing CO_2 to compete with, and eventually surpass, the efficiencies of hydrofluorocarbon (HFC) cycles have been conducted. Unique thermo-physical properties of CO_2 were discussed by Kim et al. (2004), where the intricacies of transcritical operation were identified. In particular, the rejection of heat in the supercritical region decouples temperature and pressure as they become independent, intensive properties outside of the two-phase region, making the heat rejection process gas cooling instead of condensing, resulting in gas cooling pressure becoming an optimizable parameter that results in a maximum coefficient of performance (COP) for a given operating condition.

A significant number of cycle modifications have been proposed to increase the COP of transcritical CO_2 cycles, and within this topic, expansion work recovery has proven to have significant potential (Ma et al., 2013). One of the most widely used methods of expansion work recovery is an ejector, which was first introduced by Gay (1931). The past decades have brought about a large amount of numerical and experimental research on ejectors (Kemper, G.A., Harper, G.F., Brown, 1996; Liu et al., 2012a; Lucas and Koehler, 2012; Newton, 1972). However, because the primary purpose of an expansion device in a vapor compression cycle is cycle control, active control of the ejector has

* Corresponding author.
E-mail address: gabriele.toffoletti@uniud.it (G. Toffoletti).

https://doi.org/10.1016/j.ijrefrig.2024.10.001
Received 18 March 2024; Received in revised form 30 August 2024; Accepted 3 October 2024
Available online 16 October 2024

Nomenclature

d	Diameter (mm)
h	Specific enthalpy ($kJ \cdot kg^{-1}$)
m	Mass (kg)
$\dot{m}$	Mass flow rate ($kg \cdot s^{-1}$)
P	Pressure (kPa, bar)
$\dot{Q}$	Heat transfer rate (kW)
s	Specific entropy [$kJ \cdot (kg\text{-}K)^{-1}$]
T	Temperature (°C, K)
U	Uncertainty (various)
V	Volume (m^3)
$\dot{V}$	Volumetric flow rate ($m^3 \cdot hr^{-1}$)
w	Entrainment ratio (-)
$\dot{W}$	Power (kW)
x	Quality (-)

Greek symbols

η	Efficiency (-,%)

Subscript

comp	Compressor
cool	Cooling capacity
d	Ejector diffuser outlet
I	Iteration counter
EG	Ethylene Glycol
ref	Refer to refrigeration cycle
mi	Ejector motive nozzle inlet
motive	Ejector motive nozzle
out	Outlet
si	Ejector suction nozzle inlet
suction	Ejector suction nozzle
X	Measured quantity
Y	Calculated quantity
1,2,3…	State points

Acronyms

COP	Coefficient of Performance
CO_2	Carbon Dioxide
EG	Ethylene Glycol
EXV	Electronic Expansion Valve
FS	Full Scale
FT	Flash Tank
GC	Gas Cooler
GWP	Global Warming Potential
HFC	Hydrofluorocarbon
HP	High Pressure
IHX	Internal Heat Exchanger
LP	Low Pressure
LT	Low Temperature
MT	Medium Temperature
P&ID	Piping and Instrumentation Diagram
RDG	Reading
VFD	Variable Frequency Drive

become a research focus. Elbel and Hrnjak experimentally investigated an ejector with a variable-diameter motive nozzle (Elbel and Hrnjak, 2008a), resulting in COP and cooling capacity improvements of 7 % and 8 %, respectively, as well as proving the device control could be used to vary the gas cooling pressure of the cycle to achieve a maximum COP. Another strategy for ejector control is the multi-ejector, introduced by Hafner et al. (2014) and experimentally investigated by Haida et al. (2016). In the latter work, COP and exergetic efficiency benefits of 7 % and 13.7 %, respectively, were obtained and cycle stability was validated through variation of both ambient temperature and flash tank pressure. Zhu and Elbel (2018) found that introducing a tangential flow upstream of a converging-diverging nozzle to impart a swirl could be an effective method to control nozzle performance. Additionally, there has been considerable research on subcooling techniques applied at the gas cooler outlet in transcritical CO_2 refrigeration systems. These studies have demonstrated that significant enhancements can be achieved overall, using the internal heat exchanger (IHX), which is one of the most commonly used enhancement (Yu et al., 2019), increments in COP of up to 12 % (Torrella et al., 2011), using economizers (subcooling by expanding a part of the liquid) up to 21 % (Cavallini et al., 2005) and using an external vapor compressor cycle known as dedicated mechanical subcooler (DMS) up to 29 % (from 1.51 to 1.95) with an additional increase of 1.5 % if a zeotropic mixture is used in the DMS, respectively (Llopis et al., 2021; Nebot-Andrés et al., 2021) compared to the base CO_2 cycle. The use of non-azeotropic mixtures can have improvements not only when used in DMS, but when used in the primary cycle: the so-called CO_2-based mixtures (Yu et al., 2019). In particular, (Martínez-Ángeles et al., 2023) evaluated a performance improvement of 6.9 % theoretically and of 7.3 % experimentally (Sicco et al., 2024) with a mixture CO_2/R-152a [90/10 %] compared to the pure CO_2 cycle.

Multi-evaporator cycles are commonly applied in both supermarket and transport refrigeration due to the need to maintain cooling compartments at different temperatures while using a central vapor compression cycle. To offer a transportation container refrigeration perspective, Lawrence et al. (2018) numerically assessed the performance of a multi-temperature refrigerated transportation container system using a transcritical CO_2 with an ejector and internal heat exchanger, resulting in a COP of 0.96 at an extreme ambient temperature of 57 °C. Barta et al. (2018) also investigated a multi-temperature refrigeration container system numerically, applying an expander and a flash tank upstream of the medium temperature (MT) evaporator, achieving a COP of 1.28 at an ambient temperature of 57.2 °C. These papers numerically displayed the ability of complex cycles to be applied to multi-evaporator transportation container refrigeration systems in an effort to achieve COP values equal to or over unity, motivating further experimental investigation. The cycle architectures applied in transcritical CO_2 supermarket applications vary in complexity in order to achieve performance benefits over the HFC cycles they seek to replace, depending on the proposed ambient conditions (Karampour and Sawalha, 2018). On the complex end of this spectrum, Minetto et al. (2014) experimentally investigated parallel compression, ejector expansion work recovery, and flooded evaporation in a multi-evaporator architecture, reducing compressor power consumption by 13 % at an ambient temperature of 16 °C. Numerous technical approaches can be employed to enhance the energy efficiency of the fundamental booster CO_2 system, striving to achieve energy performance at least on par with conventional HFC-based plants. The literature contains various publications that offer comparisons among different solution alternatives. Gullo et al. (2017) theoretically evaluated the multi-ejector concept where a drop in energy consumption by 19.4 % over an R-404A system is calculated and a potential energy saving of 15.6 % can be achieved if integrated CO_2 solution were used. Sawalha (2008) achieved a COP improvement of 3–7 % over the temperature range of 10–40 °C among some possible modifications (parallel, cascade and centralized modified) and improvement on the CO_2 systems solutions for supermarket refrigeration compared to R-404A. A review which provides numerous examples of multi-evaporator architectures, expansion work recovery, and phase separation was written by

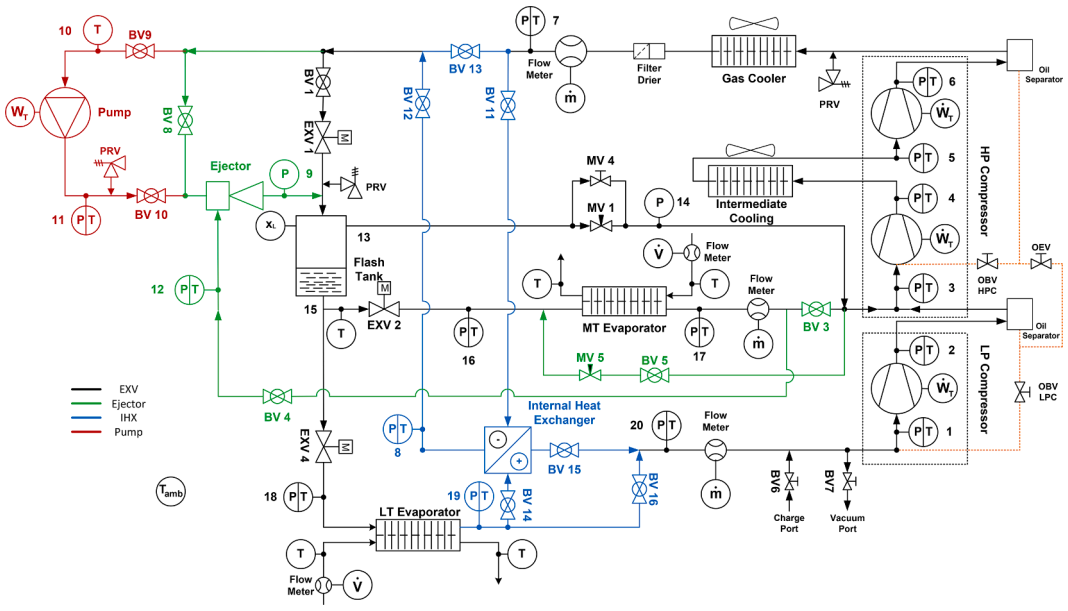

Fig. 1. P&ID of the utilized test stand.

Table 1
Components used in test stand.

Equipment	Manufacturer	Model	Tech. info
HP Compressor	Carlyle	06V	$V = 33.3\ cm^3 + 20.0\ cm^3$
LP Compressor	Dorin	CD300H	$V = 16.7\ cm^3$
Gas cooler	Custom	Microchannel HX	3 in series (5 kW each)
MT Evaporator	Swep	SS B16×26	$A = 0.928\ m^2$
LT Evaporator	Swep	SS B16×24	$A = 0.880\ m^2$
IHX	Swep	B18Hx10/1P	$A = 0.328\ m^2$
EXV1	Danfoss	CCMT4	$Kv = 0.45\ m^3\ hr^{-1}$
EXV2	Danfoss	CCMT4	$Kv = 0.45\ m^3\ hr^{-1}$
EXV4	Danfoss	CCMT2	$Kv = 0.18\ m^3\ hr^{-1}$
Ejector	Custom	Variable diameters	15 kW nominal capacity (Liu et al., 2012b)
CO_2 Pump	Hammelmann	HAMPRO-12	$\dot{V} = 12.16$ l/min at 500rpm
Flash Tank	Refrigeration Research	3370	$V = 8.34$ l

Gullo et al. (2018) for additional reference. Finally, the multi-stage and open-economization combination with an ejector was informed by Ladd (2019a, 2019b, 2019c, 2018) with the intention of validating a particular multi-stage flashing refrigeration cycle as well as use of a pump to increase the performance of the ejector.

Despite the significant amount of research that has been conducted on enhancing the performance of transcritical CO_2 refrigeration cycles, there are still limited studies that cover experimental investigations of multiple cycles compared with the same experimental setup, nor are there any papers which considered the use of a CO_2 pump as a method to control the ejector. This paper presents a comprehensive experimental comparison of four cycle architectures for a multi-stage two-evaporator transcritical CO_2 refrigeration cycle. The experimental investigation using a pump to control the CO_2 ejector cycle is based on the principle conducted by Barta et al., (2021a). Among the cycle comparisons are two methods for ejector control. The first control method is a variable motive nozzle and the second is the addition of a variable-speed pump located at the gas cooler outlet to vary the ejector motive nozzle inlet pressure. The results of a comprehensive comparison parametric study are presented, as is an assessment of the effectiveness of both proposed control methods.

2. System overview

2.1. Test stand design

The experimental test stand utilized in this work (Fig. 1) features two evaporation temperatures, three stages of compression, intercooling between the second and third compression stages, a flash tank at the medium-temperature (FT) evaporator inlet, an IHX, a CO_2 pump located between the gas cooler outlet and ejector motive nozzle inlet, and either an electronic expansion valve (EXV) or an ejector for expansion. An ejector (Fig. 3) harnesses expansion work by accelerating the high-pressure flow from the gas cooler outlet via a motive nozzle into a high-velocity motive flow, which entrains low-pressure flow from the evaporator outlet through a suction nozzle. The two flows then mix and diffuse at a pressure higher than the evaporation pressure, which reduces the amount of pressure lift required of the compressor and thus, the required compressor input power. In this work, the back pressure valve and the ejector are never used simultaneously, so switching from one configuration to another has to be done manually using several ball valves. Open economization is conducted with a flash tank, which is a large vessel. Two phase flow enters the flash tank and flashed into separate phases because of the sudden increase in volume. Gravity then further separates the liquid and vapor phases such that the saturated vapor flows out the top of the tank to bypass the evaporator and enters

Table 2
Experimentally investigated cycle configurations.

Configuration 1	EXV + Flash Tank Economization
Configuration 2	Ejector
Configuration 3	EXV + Flash Tank Economization + IHX
Configuration 4	Ejector + IHX + CO_2 Pump

the compressor directly while the saturated liquid exits the bottom of the tank and flows through the expansion valve to enter the evaporator at a lower specific enthalpy than the evaporator would receive without the use of a flash tank. This can result in an increased cooling capacity if the impact of the larger change in specific enthalpy across the evaporator outweighs the disadvantage of the reduced mass flow rate passed through the evaporator. The list of components is presented in detail in the Table 1.

In this work, four cycle configurations were assessed over a range of operating conditions, as summarized in Table 2:

- *Configuration 1 "Baseline EXV cycle"*: This cycle implements an EXV as expansion valve with a flash tank applied upstream of the MT evaporator to facilitate open economization, where saturated liquid is throttled to the evaporator inlet and the vapor bypasses the evaporator.
- *Configuration 2 "Ejector Cycle"*: Instead of using an EXV, an ejector is operated with motive flow from the gas cooler outlet and suction flow from the MT evaporator outlet by closing BV3 valve. The ejector diffuser outlet flow then enters the flash tank, where the same open economization process as in configuration 1 takes place occurs.
- *Configuration 3 "EXV and IHX cycle"*: This cycle is similar to the baseline cycle (*Configuration 1*), but an IHX is utilized to further cool the gas cooler outlet flow before it is expanded into the flash tank and also to further superheat the compressor suction flow.
- *Configuration 4 "Ejector, IHX and pump cycle"*: This is the most complex cycle using both ejector and IHX with an additional CO_2 pump added between the gas cooler outlet and the motive nozzle inlet to increase the cycle efficiency by providing additional pressure differential across the motive nozzle and thus, additional potential work for expansion work recovery.

The reasoning behind employing a pump is that less work is required to increase the pressure of a liquid than a gas due to the smaller change in specific volume for a given pressure rise due to the less-compressible fluid states. Therefore, the work required by the pump would result in an increase in ejector pressure lift, and, theoretically, decrease the work input required by the compression process by a larger amount than was consumed by the pump. A further advantage of the pump is to facilitate modulation of the motive nozzle input state to provide control of the ejector efficiency, pressure lift, and entrainment ratio without needing variable ejector geometry. The volumetric CO_2 pump used in this work is an HAMMELMANN High Pressure Process pump with a capacity of 12.16 l/min at 500 rpm with the discharge line at the top and the suction line at the bottom (Fig. 2). The ejector utilized in this work was developed and tested by Liu et al. (2012a), and the motive nozzle diameter was varied manually during testing through rotation of a threaded needle which moved in and out of the motive nozzle throat, actively varying the effective motive nozzle flow diameter (L1 and L2 in Fig. 3); Moreover the main technical drawings of the ejector are attached in Appendix A. A piping and instrumentation diagram (P&ID) of the test stand utilized in this work is shown in Fig. 1, and a photo of the pump installed in the test stand is shown in Fig. 2.

A detailed explanation regarding the test stand development, instrumentation, and validation of the evaporator energy balance can be found in (Barta et al., 2021b). The ambient conditions are controlled with the psychrometric chamber where the test stand is located, and both evaporators are controlled by independent Ethylene-Glycol (EG) baths.

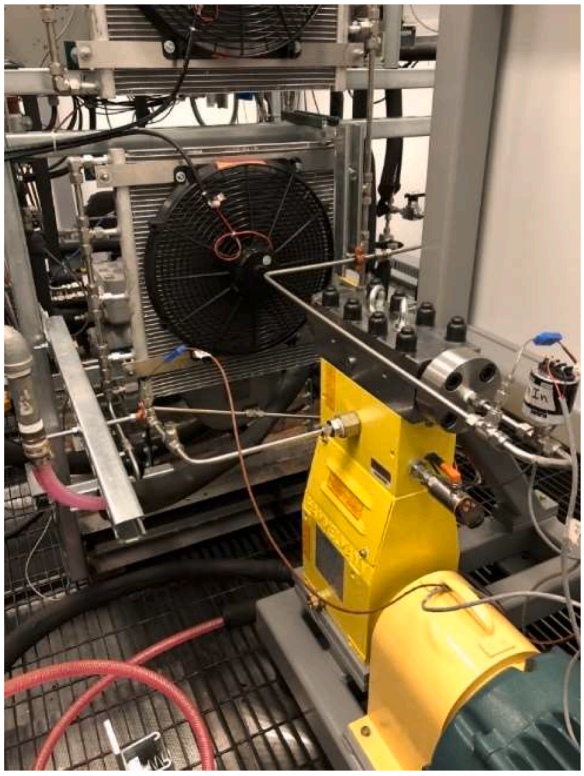

Fig. 2. Photo of the pump installed in the CO_2 test stand.

2.2. Measurement and instrumentation

All single-phase states were measured using calibrated in-line thermocouples and pressure transducers. Whereas the two-phase states were assessed with both temperature and pressure for redundancy. Three Coriolis mass flow meters were used to measure refrigerant mass flow rates, and a turbine flow meter was placed in each EG loop to measure volumetric flow rates. The EG temperature was measured at the inlet and outlet of each evaporator with in-line thermocouples placed in the EG flow. Mass concentrations of 34 % and 50 % EG were utilized in the MT and LT temperature baths, respectively. Both compressors and the pump were controlled with variable frequency drives (VFD), and the power consumption for each device was measured between the power source and the VFD. Fan power for the intercooler and gas coolers was measured via watt transducer. The flash tank liquid level was monitored by both a sight glass and capacitive liquid level sensors to pass the liquid level signal to the data acquisition system. The P&ID shown in Fig. 1 provides a visual reference for the location of the measurement devices, and details of the various measurements are provided in Table 3.

Instrumentation uncertainties are used to determine the uncertainty of calculated variables as in Eq. (1) from Taylor and Kuyatt (1994).

$$U_Y = \sqrt{\sum \left(\frac{\partial Y}{\partial X_i} U_{x_i}\right)^2} \quad (1)$$

where Y is the calculated quantity, X is the measured quantity, and U is the uncertainty (Barta et al., 2021b).

3. Cycle performance comparisons

3.1. Experimental procedure

The experimental campaigns resulted in a total of 53 steady-state

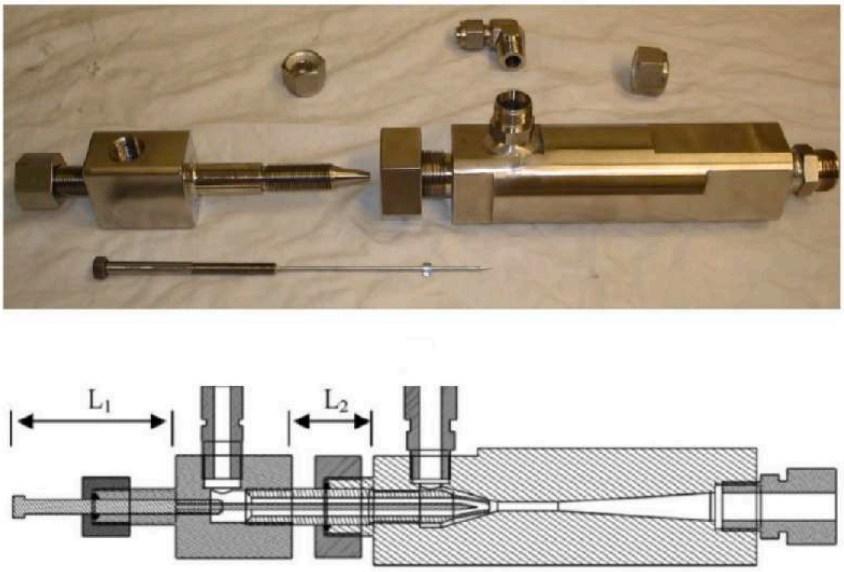

Fig. 3. Photo of the adjustable ejector with technical drawing of the ejector (Liu et al., 2012b).

Table 3
Summary of sensors and corresponding uncertainty.

Physical Parameter	Description	Model	Accuracy
Temperature	Ungrounded TC	Omega T-Type	± 0.5 K
Pressure (HP Side)	PT, 0–20,684 kPa	Setra 206	± 26.9 kPa
Pressure (LP Side)	PT, 0–6895 kPa	Setra 206	± 9.0 kPa
Mass Flow ($\dot{m}_{motive}$)	Coriolis Flow Meter	Micromotion CMFS050	± 0.1 % RDG
Mass Flow ($\dot{m}_{suction}$)	Coriolis Flow Meter	Micromotion F025	± 0.2 % RDG
Mass Flow ($\dot{m}_{LT}$)	Coriolis Flow Meter	Micromotion F025	± 0.2 % RDG
Volume Flow ($\dot{V}_{EG}$)	Turbine Volume Flow Meter	Omega FTB-1424	± 0.1 % FS
Liquid Level	Capacitive Liquid Sensor	SWI CS02	± 0.5 % Linearity
Compressor Power	Watt Transducer	Ohio Semitronics GW5–015E	± 0.2 % RDG ± 0.04 % FS
Fan Power	Watt Transducer	Ohio Semitronics PC8–001	±1.0 % FS

data points across the different cycle architectures. Steady-state points have been identified by ensuring temperature and pressure deviations from the set-points within ±0.3 K (±0.3 K if ambient temperature) and ±0.3 bar, respectively, and each data point has been obtained by averaging between five to ten minutes of steady measurement. In every test, the gas cooler pressure was varied to find the optimal pressure that resulted in the maximum COP at each ambient condition. The back pressure was regulated with an EXV using an in-house developed PID controller and implemented within the monitoring system.

Experimental tests were conducted at ambient temperatures of 19 °C (when the CO_2 pump is in operation) 24 °C, 28 °C and 30 °C, and the fans, three of which were used for the gas-cooler and one for the intercooler, were kept at a fixed speed. The heat load was provided by two EG baths: one evaporator inlet temperature target was 3 °C to simulate refrigeration applications (MT), and the low-temperature (LT) EG-side evaporator inlet temperature target was −21 °C to simulate freezer applications. Both EG flow rates were set to 10 liters per minute to maintain a proper temperature difference from inlet to outlet that would reduce the impact of the thermocouple uncertainty while still falling within the turbine flow meter measurable range. The applied test matrix is provided in Table 4. Ambient relative humidity was set at 30 % to avoid large amounts of ice buildup and a target compressor suction superheat of approximately 15 K was chosen. When the ejector is used, 15 K refers to the superheating at the outlet of the MT evaporator. When testing the plant in Configurations 3 and 4, where the IHX is used, the superheating at the LT evaporator outlet is set at 10 K in order to avoid excessive LP suction compressor superheating and to maximize the benefit of the IHX. The somewhat high superheat values were selected due to insufficient volume for mixing of the MT evaporator outlet and the first stage compressor outlet flow before the suction to the second stage compressor. Lower compressor suction superheat values led to instabilities in some investigated architectures due to notable reductions in evaporator outlet superheat values. In order to be as consistent as possible between all investigated architectures, we used a consistent

Table 4
Overview of conducted tests.

Test	Description	Ambient Temperature [°C]
1	Baseline - EXV, FT Economization	24
2	(Configuration 1)	28
3		30
4	Ejector (Configuration 2)	24
5		28
6		30
7	IHX, FT Economization (Configuration 3)	24
8		28
9		30
10	Ejector, IHX, CO_2 Pump (Configuration 4)	19

Table 5
Test stand peripheral operating parameters.

Parameter	Units	Values
LT suction (evaporator outlet) superheat	[K]	15, (10) if IHX
MT suction (evaporator outlet) superheat	[K]	15, (15) if Ejector
Ambient Temperature	[°C]	19, 24, 28, 30
Ambient relative humidity	[-]	30 %
Ethylene-Glycol inlet temperature, LT evaporator	[°C]	−21
Ethylene-Glycol inlet temperature, MT evaporator	[°C]	3
Ethylene-Glycol volumetric flow rate, LT evaporator	[l/min]	10
Ethylene-Glycol volumetric flow rate, MT evaporator	[l/min]	10
Flash Tank Pressure (open economization)	[bar]	35

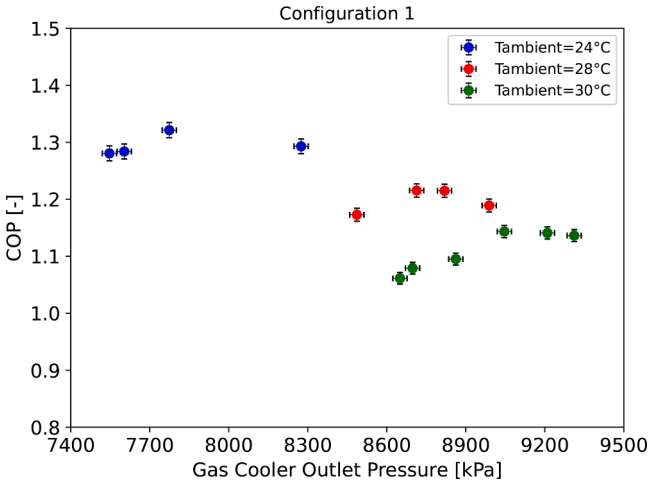

Fig. 4. Configuration 1 (Baseline, EXV with FT economization) COP with gas cooling pressure variation.

superheat value throughout all tests to ensure a fair comparison. This resulted in a somewhat high superheat, higher than what typical supermarkets operate with, applied for experimental purposes. Consequently, the absolute COP values are somewhat impacted. The system refrigerant charge was held constant at a value of 7.9 kg for all tests. In all the test conducted where open economization was achieved, the pressure in the flash tank was fixed at 35 bar via the flash gas valve in order to simulate a common supermarket refrigeration plant (Cortella et al., 2020). A summary of the cycle parameters is presented in the Table 5.

Configuration 4 (with the CO_2 pump) was tested only at an ambient temperature of 19 °C, the reasons for which will be discussed in-depth in the following section.

The calculation of key performance metrics is calculated as was done in (Barta et al., 2021b), with COP shown in Eq. (2).

$$COP = \frac{\dot{Q}_{cool,LT} + \dot{Q}_{cool,MT}}{\dot{W}_{comp,LP} + \dot{W}_{comp,HP} + \dot{W}_{pump} + \dot{W}_{fans}} \quad (2)$$

Where $\dot{Q}_{cool,LT}$ and $\dot{Q}_{cool,MT}$ are the cooling capacity from the LT and MT evaporators on the refrigerant side, respectively. In the denominator, the power consumption of the low-pressure compressor, high-pressure compressor, CO_2 pump, and fans are considered with the aim of having a COP closer to real supermarket applications with gas-cooler fans. The power consumption of water/EG pumps is neglected, and no additional electrical power is added, for example to simulate an application with air-source evaporators, where an additional fan power consumption could be considered.

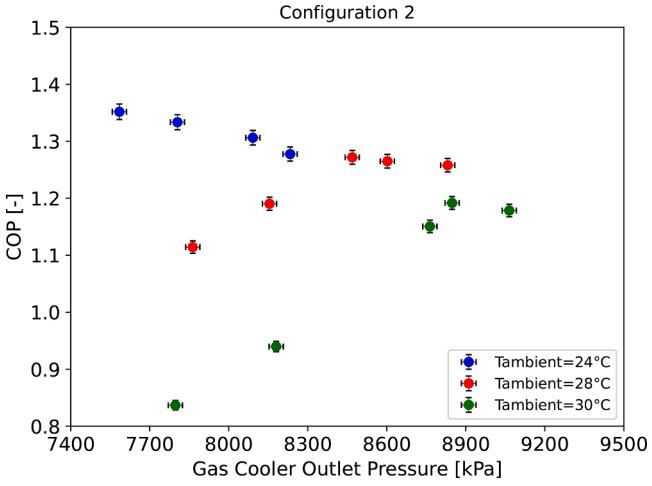

Fig. 5. Configuration 2 (Ejector) COP with gas cooling pressure variation.

3.2. Experimental results

In all the tested configurations, conditions that corresponded to a maximum COP have been identified and the resulting COP values with gas cooling pressure variation for Configurations 1, 2 and 3 at three ambient conditions are shown in Fig. (4–6), respectively.

For each configuration tested at three different ambient conditions, an optimal gas cooler outlet pressure can be identified to maximize the system COP. The COP trends followed the expected result of attaining a maximum value for a given ambient condition at a higher pressure with increasing ambient temperature. The gas cooler outlet pressure that corresponds to the maximum COP is clear for all configurations. At 24 °C, the minimum pressure is fixed at 75 bars to avoid the vapor dome and, regarding Configuration 3 at 30 °C, the maximum pressure (93 bar) is taken as optimum pressure even though an optimum was not reached

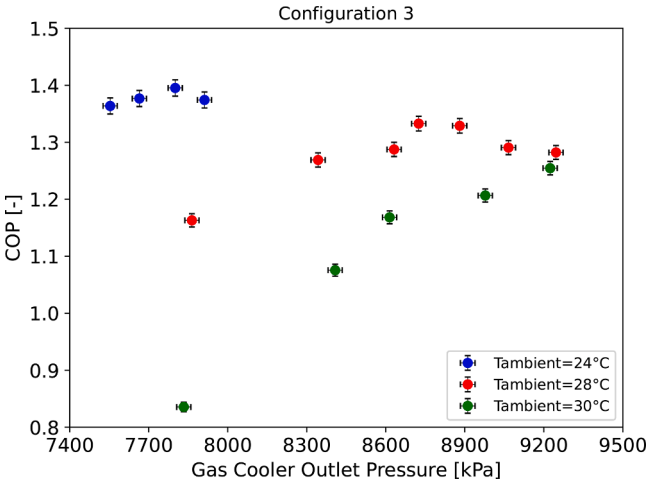

Fig. 6. Configuration 3 (IHX with FT economization) COP with gas cooling pressure variation.

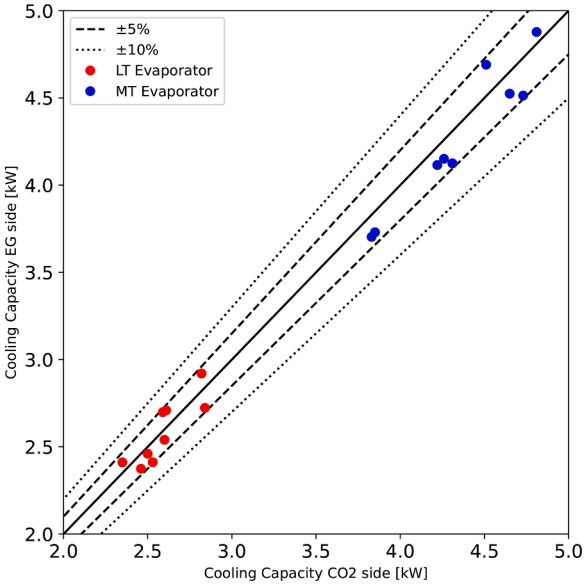

Fig. 7. LT and MT evaporator energy balance validation.

Table 6
Summary of data with and without CO_2 pump.

T_{Amb} [°C]	Architecture [-]	$P_{GC,out}$ [kPa]	$P_{pump,out}$ [kPa]	rpm [r/min]	COP [-]	$\dot{Q}_{cool,LT}$ [kW]	$\dot{Q}_{cool,MT}$ [kW]	$\dot{W}_{comp,LP}$ [kW]	$\dot{W}_{comp,HP}$ [kW]	$\dot{W}_{pump}$ [kW]
19	Ejector + IHX	6987.2 ± 26.9	–	–	1.510 ± 0.016	2.760 ± 0.008	4.700 ± 0.012	0.980 ± 0.032	3.390 ± 0.032	–
	Ejector + CO_2 Pump	7085.4 ± 26.9	7481.3 ± 26.9	125	1.460 ± 0.014	2.630 ± 0.008	5.170 ± 0.012	0.960 ± 0.032	3.430 ± 0.032	0.380 ± 0.032
	Ejector + CO_2 Pump	7047.2 ± 26.9	7971.3 ± 26.9	130	1.470 ± 0.014	2.580 ± 0.008	5.350 ± 0.012	0.970 ± 0.032	3.410 ± 0.032	0.430 ± 0.032
	Ejector + CO_2 Pump	7015.3 ± 26.9	8320.1 ± 26.9	140	1.470 ± 0.014	2.500 ± 0.008	5.480 ± 0.013	0.990 ± 0.032	3.410 ± 0.032	0.470 ± 0.032
	Ejector + CO_2 Pump	7005.7 ± 26.9	8985.6 ± 26.9	155	1.480 ± 0.014	2.580 ± 0.008	5.610 ± 0.013	1.010 ± 0.032	3.410 ± 0.032	0.560 ± 0.032
	Ejector + CO_2 Pump	6987.8 ± 26.9	9554.8 ± 26.9	170	1.460 ± 0.014	2.560 ± 0.008	5.650 ± 0.013	1.020 ± 0.032	3.410 ± 0.032	0.640 ± 0.032

due to limits on the maximum safety pressure at the gas cooler. Nevertheless, at this point there is still an improvement in COP compared to the other configurations, consistent with the tests conducted at ambient temperatures of 24 °C and 28 °C. Therefore, the improvement could potentially be greater, but it is limited by safety conditions at the gas-cooler in this specific system. From this point onwards, each configuration analysis was conducted at the gas cooler pressure which results in the maximum COP. The validation of both evaporators (MT and LT) with EG-side capacities of these experimental points is shown in Fig. 7. The mean absolute errors are 3.1 % and 3.4 % for the MT and LT evaporators, respectively and the uncertainty is not represented because it would not be discernible due to the graphical scale. However, the uncertainties associated with these datapoints are provided in Table 6.

The logarithmic pressure-specific enthalpy (P-h) diagrams achieving the maximum COP at investigated ambient temperatures for Configurations 1, 2 and 3 are presented in Figs. (8–10) respectively. The maximum COP values for each configuration and the corresponding gas cooler outlet pressure at three different ambient temperatures are plotted in Fig. 11 for an overall comparison.

The ejector was originally sized for a 15 kW air conditioning system, and was therefore oversized for the test stand at refrigeration conditions, as the test stand utilized herein has an approximate total cooling capacity of 8 kW. This led to reduced ejector efficiency, but the motive nozzle was still able to be modulated to provide adequate control of the gas cooling pressure. Compared with Configuration 1 as baseline, Configuration 2 improves the system COP for all investigated conditions, which also allowed the optimum gas cooler outlet pressure to be lowered by 1.9 bar, 2.45 bar and 3.62 bar at 24 °C, 28 °C and 30 °C ambient conditions, respectively. The maximum COP improvement was found to be 2.33%, 4.64% and 3.67% at 24 °C, 28 °C and 30 °C ambient conditions, respectively. In this specific test stand, the configuration with the highest increase efficiency was Configuration 3. Using the IHX leads to COP increases of 5.60%, 9.47%, and 8.89% at 24 °C, 28 °C and 30 °C, respectively. The effect at 30 °C ambient condition is still positive, but not as much as might be expected, since, in those conditions, the tested pressure at the gas cooler was limited to approximately 92 bar. This limitation is due to the safety valve in the test stand being set at a maximum pressure of 95 bar, and therefore, the configurations being compared are not as meaningful as at lower temperatures conditions. It is fair to mention that the position chosen for the IHX did not allow for an appreciable optimum pressure-reducing effect due to the significant difference in specific heat capacity and mass flow rate between the flow in the high and low pressure line, which allows sub-cooling of the high pressure side by approximately 2–3 K, while, on the vapor side, a superheating of 60 K was reached. Therefore, the IHX should be applied on the MT line and not the LT line due to the higher mass flow rate in the MT line in such applications as well as in further investigations using this test stand.

For the sake of completeness, a summary of COP, MT and LT evaporator outlet, FT pressure, and gas cooler outlet pressures and temperatures, as well as cooling capacities and compressor power consumption for all points shown in Fig. 11 is provided in Table 7. With COP_{ref} referring to the refrigeration COP, without taking into account external power consumption such as fan power.

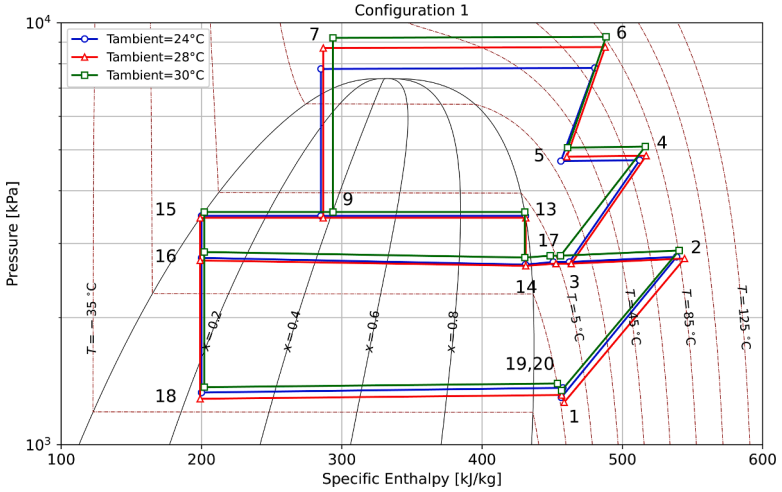

Fig. 8. P-h diagram of Configuration 1 (EXV and FT economization).

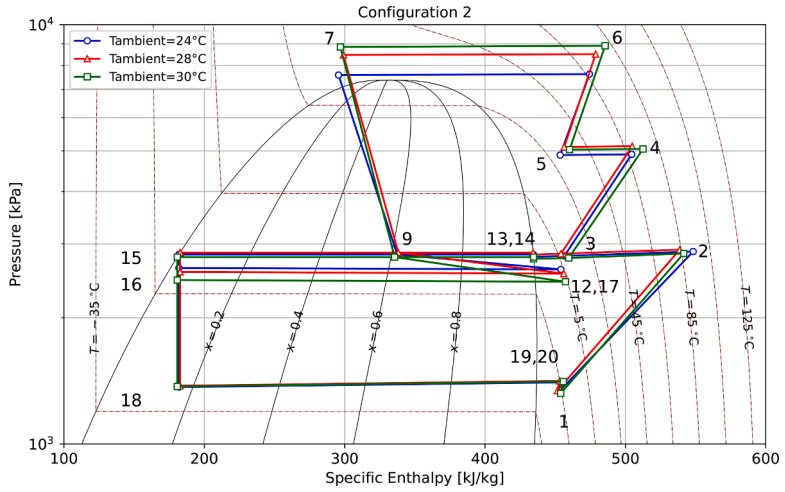

Fig. 9. P-h diagram of Configuration 2 (ejector) cycle.

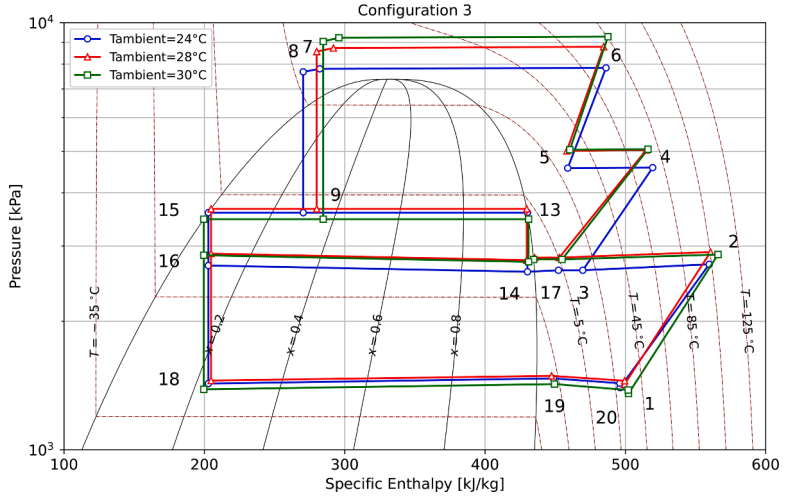

Fig. 10. P-h diagram of Configuration 3 (IHX and FT economization) cycle.

4. Ejector control and performance assessment

Two methods of ejector control were assessed in this work. The first was a variable-diameter motive nozzle and the second was a variable-speed pump located between the gas cooler outlet and motive nozzle inlet.

An energetic and ejector performance analysis of the variable-diameter method is presented herein, followed by a dedicated section with the performance of the pump method with the aim of achieving the required parameters for the safe operation of the CO_2 pump. To evaluate the ejector performance, entrainment ratio, w, and ejector efficiency, η_{ejector}, are utilized, as defined in Eqs. (3) and (4), respectively (Elbel and Hrnjak, 2008b).

$$w = \frac{\dot{m}_{\text{suction}}}{\dot{m}_{\text{motive}}} \tag{3}$$

where *suction* refers to the suction nozzle flow and *motive* refers to the motive nozzle flow.

$$\eta_{\text{ejector}} = w\frac{h(P_{\text{d}}, s_{\text{si}}) - h_{\text{si}}}{h_{\text{mi}} - h(P_{\text{d}}, s_{\text{mi}})} \tag{4}$$

where h is specific enthalpy, P is pressure, s is specific entropy, *si* denotes the suction nozzle inlet, *mi* denotes the motive nozzle inlet, and *d* denotes the ejector diffuser outlet. The pressure lift achieved by the ejector is defined as the difference in pressure between the ejector diffuser outlet and the MT evaporator outlet (pressure in point 17 in Fig. 1) in Eq. (5).

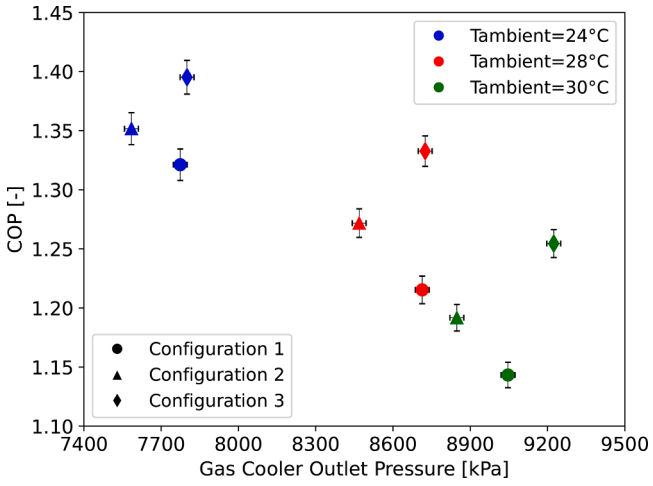

Fig. 11. Summary of maximum achieved COP for Configurations 1, 2 and 3.

Table 7
Summary of data at maximum COP conditions for all tests for Configurations 1, 2 and 3.

[°C]	Configuration [-]	$T_{gc,out}$ [°C]	$P_{LT,out}$ [kPa]	$P_{MT,out}$ [kPa]	P_{FT} [kPa]	$P_{GC,out}$ [kPa]	COP [-]	COP_{ref} [-]	$\dot{Q}_{cool,LT}$ [kW]	$\dot{Q}_{cool,MT}$ [kW]	$\dot{W}_{comp,LP}$ [kW]	$\dot{W}_{comp,HP}$ [kW]
30	1 - FT Economization	34.5 ± 0.5 K	1396 ± 9	2837 ± 9	3540.2 ± 26.9	9046.1 ± 26.9	1.140 ± 0.011	1.270 ± 0.011	2.600 ± 0.008	3.830 ± 0.011	1.010 ± 0.032	4.050 ± 0.032
	2 - Ejector	34.3 ± 0.5 K	1409 ± 9	2438 ± 9	2790.6 ± 26.9	8847.3 ± 26.9	1.190 ± 0.011	1.330 ± 0.011	2.840 ± 0.008	3.850 ± 0.010	1.040 ± 0.032	4.000 ± 0.032
	3 – IHX; FT Economization	34.9 ± 0.5 K	1426 ± 9	2829 ± 9	3490.5 ± 26.9	9224.3 ± 26.9	1.250 ± 0.012	1.400 ± 0.012	2.350 ± 0.007	4.730 ± 0.012	0.980 ± 0.032	4.100 ± 0.032
28	1 - FT Economization	32.0 ± 0.5 K	1312 ± 9	2710 ± 9	3485.6 ± 26.9	8713.4 ± 26.9	1.220 ± 0.012	1.350 ± 0.012	2.460 ± 0.007	4.220 ± 0.011	1.000 ± 0.032	3.930 ± 0.032
	2 - Ejector	33.6 ± 0.5 K	1414 ± 9	2549 ± 9	2860.8 ± 26.9	8468.1 ± 26.9	1.270 ± 0.012	1.420 ± 0.012	2.820 ± 0.008	4.260 ± 0.011	1.040 ± 0.032	3.950 ± 0.032
	3 – IHX; FT Economization	33.1 ± 0.5 K	1490 ± 9	2853 ± 9	3520.2 ± 26.9	8725.9 ± 26.9	1.330 ± 0.013	1.490 ± 0.013	2.500 ± 0.008	4.810 ± 0.013	0.990 ± 0.032	3.930 ± 0.032
24	1 - FT Economization	29.7 ± 0.5 K	1364 ± 9	2746 ± 9	3509.1 ± 26.9	7774.3 ± 26.9	1.320 ± 0.013	1.480 ± 0.013	2.590 ± 0.008	4.310 ± 0.011	1.020 ± 0.032	3.640 ± 0.032
	2 - Ejector	30.7 ± 0.5 K	1302 ± 9	2608 ± 9	2931.0 ± 26.9	7584.2 ± 26.9	1.350 ± 0.014	1.510 ± 0.014	2.610 ± 0.008	4.510 ± 0.011	1.070 ± 0.032	3.630 ± 0.032
	3 – IHX; FT Economization	29.2 ± 0.5 K	1469 ± 9	2677 ± 9	3540.7 ± 26.9	7800.1 ± 26.9	1.400 ± 0.014	1.570 ± 0.014	2.530 ± 0.008	4.650 ± 0.012	0.960 ± 0.032	3.620 ± 0.032

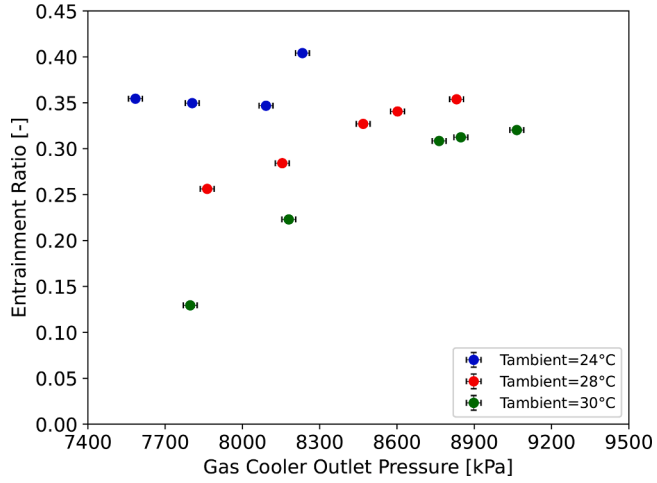

Fig. 12. Entrainment ratio with varying gas cooler pressure via motive nozzle modulation.

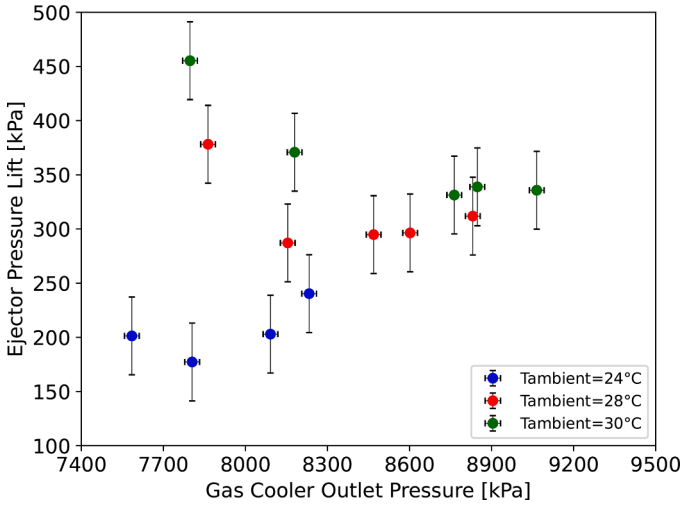

Fig. 13. Ejector pressure lift with varying gas cooler pressure via motive nozzle modulation.

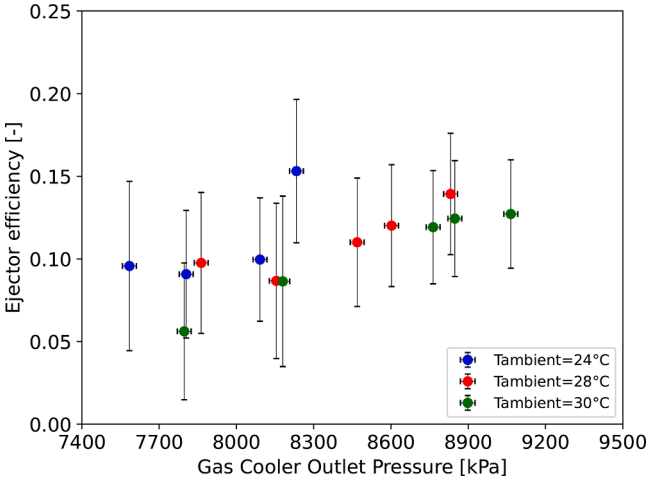

Fig. 14. Ejector efficiency with varying gas cooler pressure via motive nozzle modulation.

$$P_{\text{lift}} = P_d - P_{MT,out} \tag{5}$$

4.1. Variable diameter motive nozzle

The motive nozzle diameter variation was used to search for the gas cooler outlet pressure corresponding to the maximum COP, as shown in Fig. 5, validating motive nozzle diameter modulation as an effective means of gas cooling pressure variation. Entrainment ratio, ejector pressure lift and efficiency trends with motive nozzle modulation (i.e., gas cooler pressure) at various ambient temperature are presented in Figs. (12–14) respectively. In nearly all assessed operating points presented in Fig. 12, the entrainment ratio (0.35, 0.33 and 0.31, where the COP is maximum, at 24 °C, 28 °C and 30 °C, respectively) was observed to be directly proportional to the gas cooler pressure.

This is because the motive pressure is the driving force of the ejector, which increases the entrained flow rate from the evaporator and thus, the cooling capacity. As the gas cooler pressure increases, the motive mass flow rate typically decreases due to the inverse relationship of compressor mass flow rate to pressure ratio. Furthermore, with increasing gas cooler pressure for a given ambient condition, the motive nozzle inlet specific enthalpy decreases, thus leading to a lower motive nozzle outlet quality for scenarios where the expansion process enters

the vapor dome. Thus, the fraction of the total mass flow passing through the evaporators further increases. The combination of these trends explains the observation of the direct relation of entrainment ratio and motive nozzle inlet pressure.

The pressure lift is shown in Fig. 13 with the uncertainty calculated using the two pressure transducers in low-pressure lines. The experimental results show a direct relationship between ambient temperature and ejector pressure lift due to the larger amount of available expansion work to be recovered at higher gas cooler pressures associated with the higher ambient temperature. Looking more closely, higher pressure lift values at lower gas cooling pressures were observed, which then stabilized with the increase of gas cooler pressure for ambient temperatures of 28 °C and 30 °C, while remaining nearly constant at 24 °C ambient. The main explanation regarding this difference in behavior between higher ambient temperature (28 °C and 30 °C) and 24 °C ambient temperature is the strong dependence of ejector diffuser outlet pressure with nozzle diameter. At a temperature of 24 °C, only slight changes in ejector geometry are required to achieve conditions that maximize COP, while at higher ambient temperatures, more significant changes in ejector geometry and thus, higher diffuser outlet pressure changes are required to achieve conditions that maximize COP. This explains why pressure lift changes are more pronounced when the ejector is further from the conditions that maximize system performance, and the combination of these two parameters (shown in Figs. 12 and 13) sheds light on the ejector efficiency behavior shown in Fig. 14. Therefore, it is shown how an analysis on ejector efficiency trends must go through an analysis of entrainment ratio and pressure lift trends together and, as a result, provide the overall ejector efficiency.

Considering that the evaporator outlet superheat was fixed at 15 K, the general trend shows an increase in ejector efficiency as the pressure at the gas cooler outlet increases, with the sole exception of the test at 78.63 bar and an ambient temperature of 28 °C. This result is likely due to the high ejector pressure lift at that point that affects the efficiency calculation. It is worth mentioning that an increase in the efficiency of a single component does not always increase overall cycle efficiency. To support this statement, it can be seen that the points with the highest ejector efficiency do not necessarily correspond to the points where system COP is highest. Moreover, contrary to many expansion work recovery device control methods, this variation in diameter did not significantly impact the ejector efficiency. Finally, the uncertainty in the calculation of ejector efficiency is significantly higher than for the other quantities presented. This comes from the fact that the calculation of efficiency (Eq. 4) includes the calculation of the uncertainty associated with the specific enthalpy inlet, and this zone often is situated just above the critical point, which is associated with a nearly flat isotherm.

4.2. Variable speed CO_2 pump

Applying a pump to compress the sub-cooled liquid, where the temperature and pressure of the refrigerant are below their respective critical values, or supercritical liquid, where the fluid pressure is above the critical pressure, but the temperature is below the critical temperature, resulted in consistent trends and reliable operation. To respect the safety constraints of the pump and avoid cavitation, a maximum pump inlet temperature of 25 °C and a maximum pump discharge pressure of 100 bar are recommended by the manufacture, which results in a dedicated test condition. The manufacturer-recommended subcooling at the pump inlet is 5 K, which necessitated the use of an IHX at the gas cooler outlet. Additionally, by varying the CO_2 pump speed to control the motive inlet pressure and the ejector performance, the suction pressure of the pump, which is also the pressure at the gas cooler outlet as shown in Fig. 1, also varies with the pump speed as a secondary effect. This implies that, by increasing the pump speed, the pressure in the gas-cooler can decrease, reducing the degree of subcooling, and thus, increasing the risk of cavitation. Additionally, the pump suction temperature can increase as the pump rpm increases, making it more difficult to remain below the manufacturer limit of 25 °C. The maximum pump speed was limited to keep the pump discharge pressure below 100 bar as the maximum designed discharge pressure. For all the reasons explained above, the ambient temperature for this specific evaluation was fixed at 19 °C. With the aim of making the comparison as fair as possible, and to isolate the effect of the pump as much as possible, the pump testing (Configuration 4) is compared to the test stand with both the ejector and the IHX (Configuration 2+IHX), the comparison is evaluated with all the other parameters fixed as shown in Table 5, working in subcritical conditions with an initially-fixed gas cooler pressure of 70 bar. In accordance with the compressor envelope provided by the manufacturer, the operating point in this test with respect to the MT compressor is achievable with the only caution being to verify that the point at the first stage exit does not cross the saturation curve (Point 5 in Fig. 15) which does not occur in any of the experiments presented here.

To operate the CO_2 pump, starting from the baseline conditions with a fixed gas cooler pressure of 70 bar and an ambient temperature of 19 °C, the IHX bypass valves were opened, and the CO_2 pump was engaged with a speed corresponding to the volumetric flow at the gas cooler outlet. An example of Configuration 4 cycle on a P-h diagram is presented in Fig. 15.

Once the CO_2 pump is correctly engaged, the pump speed is increased to control ejector performance. A comparison between Configurations 4 and Configuration 2 with the IHX, with increasing pump speed and thus, motive nozzle inlet pressures up to 100 bar, was conducted. As before, the entrainment ratio, pressure lift and ejector efficiency are presented as a function of pump outlet pressure and thus, ejector motive nozzle inlet pressure, in Figs. 16, 17 and 18 respectively.

Figs. (17 and 18) show nearly linear trends as pump speed increases while the entrainment ratio (Fig. 16) increases rapidly around 75 bar and then is somewhat stable as the motive nozzle inlet pressure increases from a value of 0.38 without pump to an approximately constant average value of 0.44 when the pump is used. Another key aspect of this result is that the ejector efficiency is not adversely impacted by the pump operation, validating its use as a control mechanism to operate the cycle at optimal conditions without sacrificing component efficiency. This regulation allows an increase in cooling capacity through the use of the pump due to its direct relation to the entrainment ratio. Despite a somewhat insignificant decrease in compressor power consumption, the overall system COP increases through use of the pump. The overall pump efficiency varied from 22% to 38% during the tests. This low efficiency was due to the maximum pump operating speed being approximately 40% of the design speed for the pump. The pump was oversized due to difficulty in finding the correct pumps designed for these purposes and the desire to also be able to accommodate evaporation conditions associated with air condition operating conditions. Such a strong sensitivity to rotational speed was not expected, and therefore it is recommended that, in future investigations, different pumps are utilized for air conditioning and refrigeration applications, highlighting a challenge of developing flexible tests stands for laboratory work instead of single-application machines. Increased pump efficiency would further increase the COP benefit of the combined use of the ejector and pump. With the aim of reducing the impact of the oversized pump efficiency on the system COP, an alternative COP, COP_{mec}, is presented in Eq. (6) to offer a more general performance trend.

$$COP_{mec} = \frac{\dot{Q}_{cool,LT} + \dot{Q}_{cool,MT}}{\dot{W}_{comp,LP} + \dot{W}_{comp,HP} + \dot{m}\cdot\Delta h_{Pump} + \dot{W}_{fans}} \quad (6)$$

Where $\dot{m}\cdot\Delta h_{Pump}$ is the product of the mass flow and the specific enthalpy difference across the CO_2 pump. This COP has the meaning of a "mechanical coefficient of performance", where the pump mechanical and electrical efficiency are therefore equal to 1, this parameter represents the maximum COP that could be achieved with a perfectly sized pump without heat losses. Therefore, the goal is to isolate the effect of an

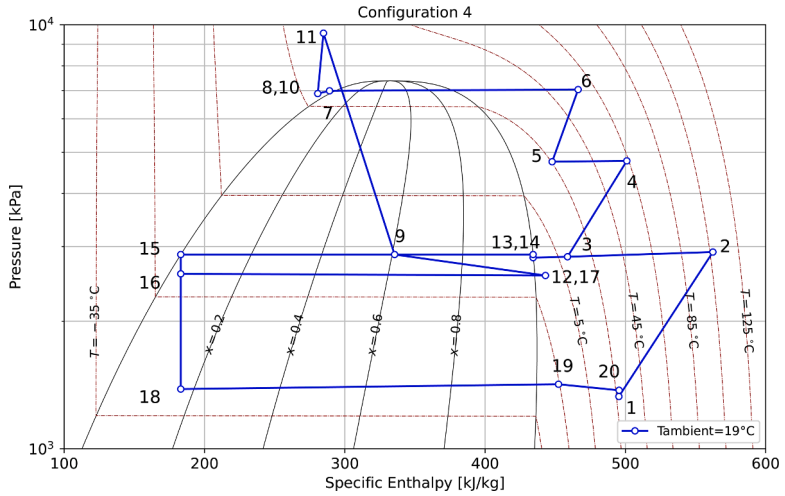

Fig. 15. P-h cycle in Configuration 4, which utilized the CO_2 pump.

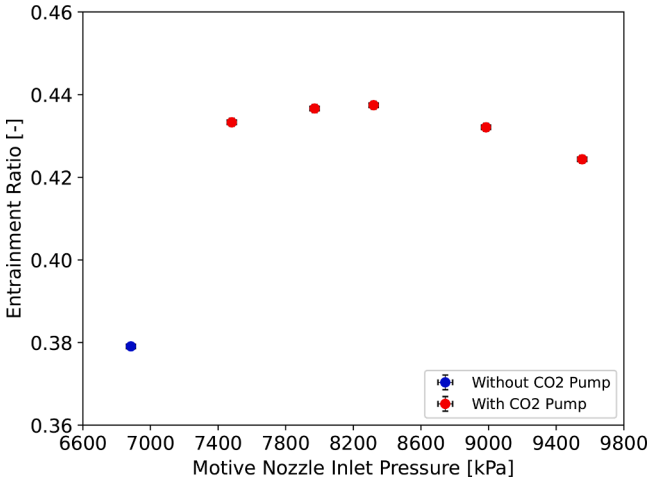

Fig. 16. Entrainment ratio with motive nozzle inlet pressure.

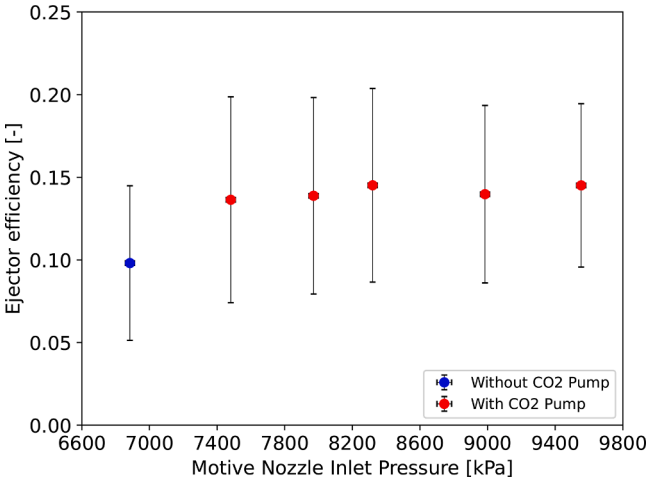

Fig. 18. Ejector efficiency with motive nozzle inlet pressure.

oversized pump as much as possible. Ideally, the mass flow should also change if the pump were perfectly sized, however by changing only the electrical power input the final COP value refers to a CO_2 flow that is not ideal but still measured and therefore more closely related to reality.

This mechanical COP result in an indication based on experimental evidence anyway even though the impact of a CO_2 pump might be higher in terms of COP. Additionally, in order to evaluate the impact of the assumed pump efficiency, two additional parameters are presented

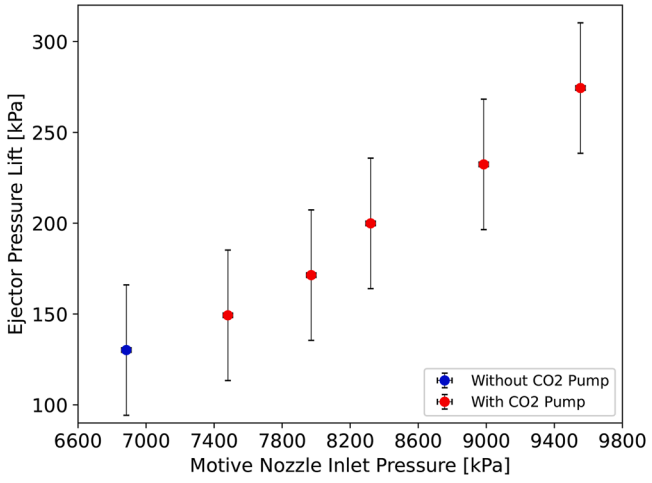

Fig. 17. Ejector pressure lift with motive nozzle inlet pressure.

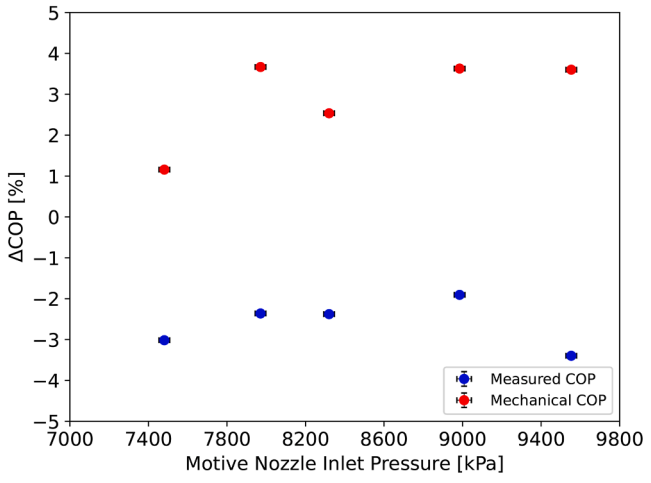

Fig. 19. Percentage difference in COP with ejector inlet pressure.

in Eqs. (7) and Eq. (8).

$$\Delta COP_{\%(\mathrm{mec})} = \frac{COP_{conf.4(mec)} - COP_{conf.2+IHX}}{COP_{conf.2+IHX}} \cdot 100 \quad (7)$$

$$\Delta \dot{Q}_{\%} = \frac{\dot{Q}_{conf.4} - \dot{Q}_{conf.2+IHX}}{\dot{Q}_{conf.2+IHX}} \cdot 100 \quad (8)$$

With $\dot{Q}$ being the overall cooling capacity and COP being the value presented in Eq. (2).

The percentage difference in COP with ejector inlet pressure is presented in Fig. 19 and a summary of measured COP, gas cooler outlet pressure, motive nozzle inlet pressure, cooling capacities, speed of the pump, compressor and pump power consumption is provided in Table 7. Uncertainty values are provided based on the uncertainty analysis conducted and are a combination of measurement uncertainty as well as error propagation. In this configuration, using the CO_2 pump leads to an increase in overall cooling capacity up to 6 % when the pump is at maximum tested speed, while the COP gradually decreases with the increase of the motive nozzle inlet pressure and thus, pump speed. This trend is justified by the fact that increasing the inlet pressure of the ejector means increasing the pump rpm and thus the consumed electrical power. Under these test conditions, the cooling capacity increase is not sufficient to compensate power consumption increase and leads to a decreasing COP. Looking at the $\Delta COP_{\%,\ \mathrm{mec}}$, the absolute values are higher due to the lower power consumption of the pump. However, the trend is not clear as the ejector inlet pressure varies. One of the major explanations is the calculation of the $\dot{m} \cdot \Delta h_{Pump}$. The change in specific enthalpy does not necessarily increase with increasing pump speed as one might expect. As pressure lift increases with rpm, the mass flow through the gas cooler increases, and this leads to an increase in the inlet temperature of the CO_2 pump of nearly 3 K. This effect influences the calculation of the specific enthalpy difference, which helps justify an unclear trend in the Fig. 19, since not only the pump performance is behind it, but also the behavior of the gas cooler and the IHX. Nevertheless, comparing the mechanical COP is of fundamental importance in understanding the impact of pump efficiency and the room for improvement. The trend of $\Delta COP_{\%(\mathrm{mec})}$, suggesting that with a perfectly sized pump, the use of a CO_2 pump to regulate ejector performance could provide appreciable benefits in terms of overall COP of maximum 3.68% in subcritical conditions.

5. Conclusions

This paper presented an experimental analysis comparing two ejector control methods and four cycle architectures applied in a two-evaporator transcritical CO_2 refrigeration cycle with an approximate cooling capacity of 8 kW. In particular, the two ejector control methods assessed were motive nozzle diameter variation via a manually-adjustable needle located in the motive nozzle throat and motive nozzle inlet pressure modulation through a variable-speed pump placed between the condenser/gas cooler outlet and the ejector motive nozzle inlet. The assessed cycles were flash tank economization applied upstream of the MT evaporator (Baseline, Configuration 1), ejector (Configuration 2), flash tank with an IHX (Configuration 3) and an IHX with an ejector and a pump upstream of the ejector motive nozzle inlet (Configuration 4). The comparisons were conducted at 24 °C, 28 °C and 30 °C ambient temperatures for Configuration 1, Configuration 2, and Configuration 3, and at 19 °C only for Configuration 4. The gas cooler outlet pressure was varied at ambient condition where a transcritical operation is required, for each cycle in an effort to identify the gas cooling pressure that resulted in the maximum COP. Ejector parameters such as entrainment ratio, efficiency, and pressure lift were also assessed.

The gas cooling pressure where the maximum COP occurred for each cycle decreased as ambient temperature decreased. Maximum COP benefits of 2.3%, 4.6% and 3.7% at 24 °C, 28 °C and 30 °C ambient conditions, respectively, were achieved with the ejector alone is used and a COP increase of 5.6%, 9.5%, and 8.9% at 24 °C, 28 °C and 30 °C, respectively, were achieved using the IHX compared to baseline.

With respect to ejector control, it was found that modulation of the motive nozzle diameter led to a maximum ejector efficiency variation of approximately 6 %. The configuration utilizing the CO_2 pump was tested at only 19 °C ambient and was found to be able to increase ejector efficiency from 10 % to 15 % relative compared to the ejector configuration under the same conditions. Furthermore, correlations between nozzle position or pump speed and ejector entrainment ratio, pressure lift, and efficiency were clearly identifiable. Therefore, both methods of ejector control were validated in their ability to control the ejector. All tests utilizing the pump resulted in a lower COP with a maximum decrease of 6.1% and a higher cooling capacity with a maximum increase of 6.2% compared to the ejector cycle without the pump. A theoretical analysis with the definition of a mechanical coefficient of performance (COP_{mec}), corresponding to a theoretical value of a perfectly sized pump, was conducted, showing a potential theoretical increase of 3.68% compared to the ejector cycle without the pump. However, the pump was only tested with the system in subcritical mode. Conducting the test under subcritical conditions eliminates the possibility of comparing this configuration in transcritical operation, where the ejector is most commonly used. Safety and inefficiency limitations resulting from oversizing preclude the appropriateness of this configuration in a real plant. At this stage of experimentation, the conclusions regarding this configuration do not definitively support the idea that a CO_2 pump can increase the efficiency of a commercial CO_2 refrigeration cycle. However, raising the evaporation temperature would increase the mass flow rate, and thus the speed of the pump required, theoretically working under more optimal conditions for the pump, opening up possible developments in air conditioning systems with the test stand utilized in this work.

Future work is to optimize both ejector and pump designs for the operating conditions and capacity of this test stand to increase the COP benefit of both cycles and to analyze results with the pump in transcritical conditions. As the safety constraints for pump operation were found to be more restrictive than anticipated, future work in this experimental facility will aim to allow the CO_2 pump to be used at higher ambient temperatures safely and with more appropriate sizing for the system capacity and operation. Additionally, the position of the IHX low-temperature flow should re-evaluated.

CRediT authorship contribution statement

Gabriele Toffoletti: Writing – review & editing, Writing – original draft, Validation, Methodology, Investigation, Formal analysis. **Riley B. Barta:** Writing – review & editing, Writing – original draft, Visualization, Validation, Methodology, Investigation, Formal analysis, Data curation, Conceptualization. **Steven M. Grajales:** Investigation, Data curation. **Haotian Liu:** Writing – review & editing, Investigation. **Davide Ziviani:** Writing – review & editing, Supervision, Project administration, Funding acquisition, Conceptualization. **Eckhard A. Groll:** Project administration, Funding acquisition, Conceptualization.

Declaration of competing interest

The authors declare that they have no known competing financial interests or personal relationships that could have appeared to influence the work reported in this paper.

Acknowledgements

The authors would like to thank the Bechtel Corporation for providing intellectual property, financial and technical support as well as the faculty and staff of the Ray W. Herrick Labs for financial and

technical support.

APPENDIX A

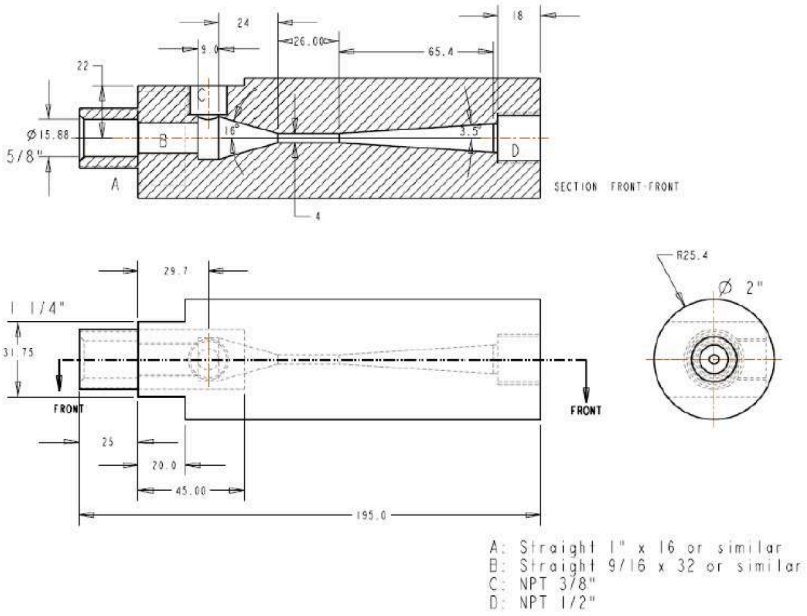

Fig. A.1. Technical drawing of the ejector: Suction nozzle, mixing and diffuser (Fang Liu and Groll, 2008).

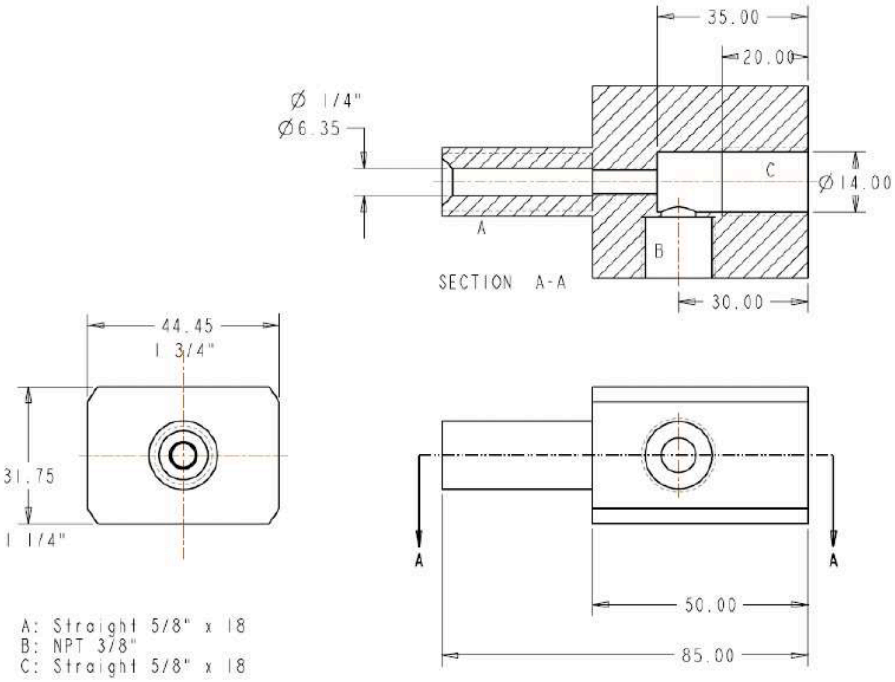

Fig. A.2. Technical drawing of the ejector: Receiving section (Fang Liu and Groll, 2008).

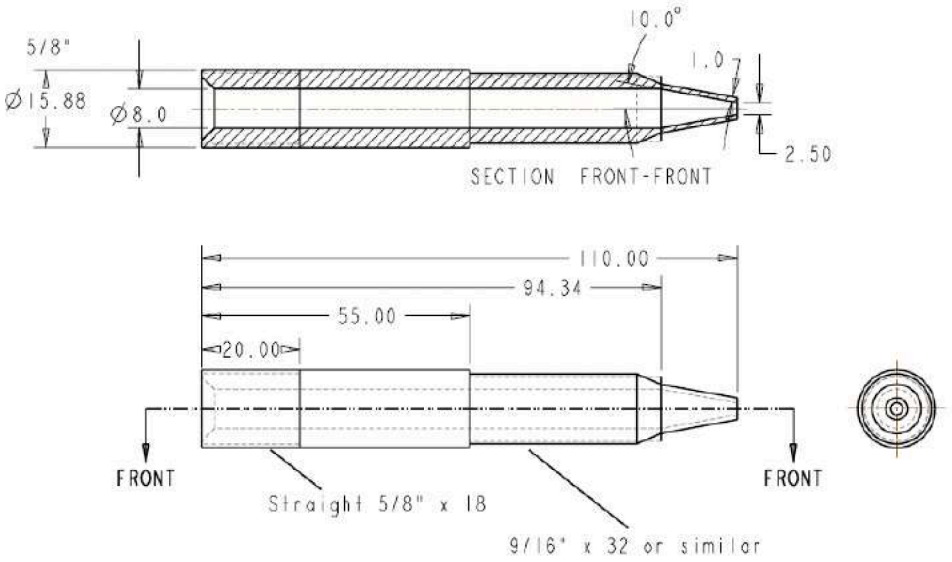

Fig. A.3. Technical drawing of the ejector: Motive nozzle (Fang Liu and Groll, 2008).

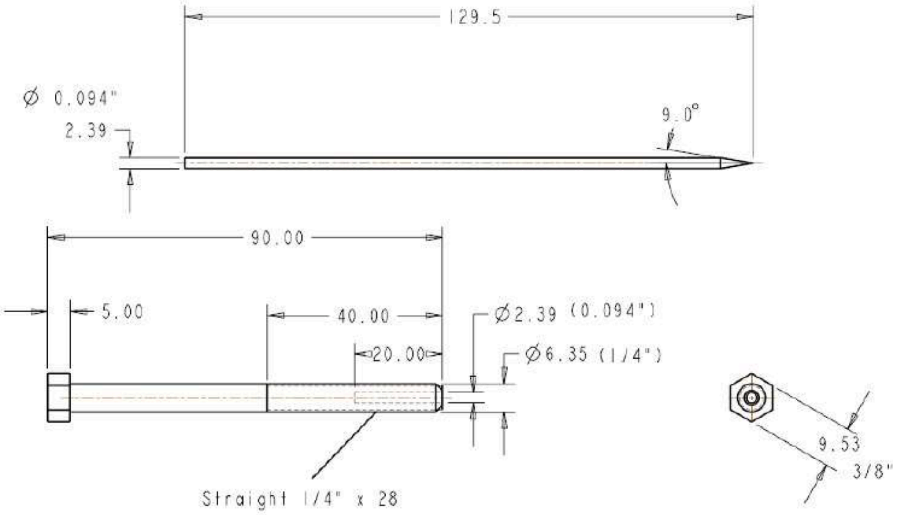

Fig. A.4. Technical drawing of the ejector: Needle (Fang Liu and Groll, 2008).

References

Barta, R.B., Hugenroth, J.J., Groll, E.A., 2018. Modeling of S-RAM energy recovery compressor integration in a transcritical carbon dioxide cycle for application in multi-temperature refrigerated container systems. In: 13th IIR Gustav Lorentzen Conference. https://doi.org/10.18462/iir.gl.2018.1117.

Barta, R.B., Beck, P.E., Ziviani, D., Groll, E.A., 2021a. Experimental Comparison of Cycle Modifications to a Multi-Stage Two-Evaporator Transcritical CO2 Refrigeration Cycle. In: International Refrigeration and Air Conditioning Conference. Paper 2096. https://docs.lib.purdue.edu/iracc/2096.

Barta, R.B., Ziviani, D., Groll, E.A., 2021b. Design and commissioning of a modular multi-stage two-evaporator transcritical CO2 test stand. Int. J. Refrig. 130, 392–403. https://doi.org/10.1016/J.IJREFRIG.2021.05.033.

Cavallini, A., Cecchinato, L., Corradi, M., Fornasieri, E., Zilio, C., 2005. Two-stage transcritical carbon dioxide cycle optimisation: a theoretical and experimental analysis. Int. J. Refrig. 28, 1274–1283. https://doi.org/10.1016/J.IJREFRIG.2005.09.004.

Cortella, G., D'Agaro, P., Coppola, M.A., 2020. Transcritical CO2 commercial refrigeration plant with adiabatic gas cooler and subcooling via HVAC: field tests and modelling. Int. J. Refrig. 111, 71–80. https://doi.org/10.1016/J.IJREFRIG.2019.11.022.

Elbel, S., Hrnjak, P., 2008a. Experimental validation of a prototype ejector designed to reduce throttling losses encountered in transcritical R744 system operation. Int. J. Refrig. 31, 411–422.

Elbel, S., Hrnjak, P., 2008b. Experimental validation of a prototype ejector designed to reduce throttling losses encountered in transcritical R744 system operation. Int. J. Refrig. 31, 411–422. https://doi.org/10.1016/J.IJREFRIG.2007.07.013.

Fang Liu, A., Groll, E.A., 2008. Recovery of throttling losses by a two-phase ejector in a vapor compression cycle Final Report.

Gay, N.H., 1931. Refrigerating System. US Patent 1,836,318.

Gullo, P., Hafner, A., Cortella, G., 2017. Multi-ejector R744 booster refrigerating plant and air conditioning system integration – A theoretical evaluation of energy benefits for supermarket applications. Int. J. Refrig. 75, 164–176. https://doi.org/10.1016/J.IJREFRIG.2016.12.009.

Gullo, P., Tsamos, K.M., Hafner, A., Banasiak, K., Yunting, T.G., Tassou, S.A., 2018. Crossing CO_2 equator with the aid of multi-ejector concept: a comprehensive energy and environmental comparative study. Energy 164, 236–263.

Hafner, A., Försterling, S., Banasiak, K., 2014. Multi-ejector concept for R-744 supermarket refrigeration. Int. J. Refrig. 43, 1–13.

Haida, M., Banasiak, K., Smolka, J., Hafner, A., Eikevik, T.M., 2016. Experimental analysis of the R744 vapour compression rack equipped with the multi-ejector expansion work recovery module. Int. J. Refrig. 64, 93–107.

Karampour, M., Sawalha, S., 2018. State-of-the-art integrated CO2refrigeration system for supermarkets: a comparative analysis. Int. J. Refrig. 86. https://doi.org/10.1016/j.ijrefrig.2017.11.006.

Kemper, G.A., Harper, G.F., Brown, G.A., 1996. Multiple Phase Ejector Refrigeration System. 3,277,660.

Kim, M.H., Pettersen, J., Bullard, C.W., 2004. Fundamental process and system design issues in CO2 vapor compression systems. Prog. Energy Combust. Sci. 30, 119–174. https://doi.org/10.1016/j.pecs.2003.09.002.

Ladd, D., 2019a. Systems and methods for multi stage refrigeration. U.S. Patent Number US 10,465,983 B2.

Ladd, D., 2019b. Systems and methods for multi stage refrigeration. U.S. Patent Number US 10,514,202 B2.

Ladd, D., 2019c. Systems and methods for multi stage refrigeration. U.S. Patent Number US 10,514,201 B2.

Ladd, D., 2018. Systems and Methods for Multi-Stage Refrigeration. U.S. Patent Number US 2018 /0231304 A1.

Lawrence, N., Elbel, S., Hrnjak, P.S., 2018. Design and validation of a transcritical CO2 mobile refrigerated container system for military applications. In: 13th IIR Gustav Lorentzen Conference on Natural Refrigerants, pp. 882–890.

Liu, F., Li, Y., Groll, E.A., 2012a. Performance enhancement of CO2 air conditioner with a controllable ejector. Int. J. Refrig. 35, 1604–1616.

Liu, F., Li, Y., Groll, E.A., 2012b. Performance enhancement of CO 2 air conditioner with a controllable ejector. https://doi.org/10.1016/j.ijrefrig.2012.05.005.

Llopis, R., Toffoletti, G., Nebot-Andrés, L., Cortella, G., 2021. Experimental evaluation of zeotropic refrigerants in a dedicated mechanical subcooling system in a CO2 cycle. Int. J. Refrig. 128, 287–298. https://doi.org/10.1016/j.ijrefrig.2021.05.028.

Lorentzen, G., 1994. Revival of carbon dioxide as a refrigerant. Int. J. Refrig. 17, 292–301. https://doi.org/10.1016/0140-7007(94)90059-0.

Lucas, C., Koehler, J., 2012. Experimental investigation of the COP improvement of a refrigeration cycle by use of an ejector. Int. J. Refrig. 35, 1595–1603.

Ma, Y., Liu, Z., Tian, H., 2013. A review of transcritical carbon dioxide heat pump and refrigeration cycles. https://doi.org/10.1016/j.energy.2013.03.030.

Martínez-Ángeles, M., Sicco, E., Toffoletti, G., Nebot-Andrés, L., Sánchez, D., Cabello, R., Cortella, G., Llopis, R., 2023. Evaluation of CO2-doped blends in single-stage with IHX and parallel compression refrigeration architectures[Évaluation de mélanges de CO2 dopés dans les architectures de refroidissement mono-étagées avec échangeur de chaleur interne (IHX) et à compression parallèle]. Int. J. Refrig. 151, 50–62. https://doi.org/10.1016/j.ijrefrig.2023.03.009.

Minetto, S., Brignoli, R., Zilio, C., Marinetti, S., 2014. Experimental analysis of a new method for overfeeding multiple evaporators in refrigeration systems. Int. J. Refrig. 38, 1–9.

Nebot-Andrés, L., Sánchez, D., Calleja-Anta, D., Cabello, R., Llopis, R., 2021. Experimental determination of the optimum working conditions of a commercial transcritical CO 2 refrigeration plant with a R-152a de dicate d mechanical subcooling. Int. J. Refrig. 121, 258–268. https://doi.org/10.1016/j.ijrefrig.2020.10.002.

Newton, A.B., 1972. Capacity Control for Multiple-Phase Refrigeration Systems. US Patent 3,670,519.

Sawalha, S., 2008. Theoretical evaluation of trans-critical CO2 systems in supermarket refrigeration. Part II: system modifications and comparisons of different solutions. Int. J. Refrig. 31, 525–534. https://doi.org/10.1016/J.IJREFRIG.2007.05.018.

Sicco, E., Martínez-Ángeles, M., Toffoletti, G., Nebot-Andrés, L., Sánchez, D., Cabello, R., Cortella, G., Llopis, R., 2024. Experimental evaluation of CO2/R-152a mixtures in a refrigeration plant with and without IHX[Évaluation expérimentale des mélanges CO2/R-152a dans une installation frigorifique avec et sans échangeur de chaleur interne]. Int. J. Refrig. 159, 371–384. https://doi.org/10.1016/j.ijrefrig.2023.12.033.

Taylor, B.N., Kuyatt, C.E., 1994. NIST Technical Note 1297 1994 Edition, Guidelines for Evaluating and Expressing the Uncertainty of NIST Measurement Results. National Institute of Standards and Technology 1–20.

Torrella, E., Sánchez, D., Llopis, R., Cabello, R., 2011. Energetic evaluation of an internal heat exchanger in a CO2 transcritical refrigeration plant using experimental data. Int. J. Refrig. 34, 40–49. https://doi.org/10.1016/J.IJREFRIG.2010.07.006.

Yu, B., Yang, J., Wang, D., Shi, J., Chen, J., 2019. An updated review of recent advances on modified technologies in transcritical CO 2 refrigeration cycle. https://doi.org/10.1016/j.energy.2019.116147.

Zhu, J., Elbel, S., 2018. Experimental investigation of a novel expansion device control mechanism: vortex control of initially subcooled flashing R134a flow expanded through convergent-divergent nozzles. Int. J. Refrig. 85, 167–183.